

CMB anisotropies at second order III: bispectrum from products of the first-order perturbations

Daisuke Nitta¹, Eiichiro Komatsu^{2,3}, Nicola Bartolo⁴, Sabino Matarrese⁴ and Antonio Riotto^{4,5}

¹ Astronomical Institute, Tohoku University, Sendai 980-8578, Japan

² Texas Cosmology Center, the University of Texas at Austin, Austin, TX 78712, USA

³ Institute for the Physics and Mathematics of the Universe (IPMU), University of Tokyo, Chiba 277-8582, Japan

⁴ Dipartimento di Fisica “G. Galilei”, Università di Padova, INFN Sezione di Padova, I-35131 Padova, Italy

⁵ CERN, Theory Division, CH-1211 Geneva 23, Switzerland

E-mail: nitta@astr.tohoku.ac.jp, komatsu@astro.as.utexas.edu, nicola.bartolo@pd.infn.it, sabino.matarrese@pd.infn.it and riotto@mail.cern.ch

Abstract. We calculate the bispectrum of the Cosmic Microwave Background (CMB) temperature anisotropies induced by the second-order fluctuations in the Boltzmann equation. In this paper, which is one of a series of papers on the numerical calculation of the bispectrum from the second-order fluctuations, we consider the terms that are products of the first-order perturbations, and leave intrinsically second-order terms and perturbations in the recombination history to the subsequent papers. We show that the bispectrum has the maximum signal in the squeezed triangles, similar to the local-type primordial bispectrum, as both types generate non-linearities via products of the first-order terms in position space. However, detailed calculations show that their shapes are sufficiently different: the cross-correlation coefficient reaches 0.5 at the maximum multipole of $l_{max} \sim 200$, and then weakens to 0.3 at $l_{max} \sim 2000$. The differences in shape arise from (i) the way the acoustic oscillations affect the bispectrum, and (ii) the second-order effects not being scale-invariant. This implies that the contamination of the primordial bispectrum due to the second-order effects (from the products of the first-order terms) is small. The expected signal-to-noise ratio of the products of the first-order terms is ~ 0.4 at $l_{max} \sim 2000$ for a full-sky, cosmic variance limited experiment. We therefore conclude that the products of the first-order terms may be safely ignored in the analysis of the future CMB experiments. The expected contamination of the local-form f_{NL} is $f_{NL}^{local} \sim 0.9$ at $l_{max} \sim 200$, and $f_{NL}^{local} \sim 0.5$ at $l_{max} \sim 2000$.

1. Introduction

Primordial non-Gaussianity is now recognized as a powerful probe of the details of the physics of inflation [1], as detection of large primordial non-Gaussianity would rule out all classes of inflation models that satisfy the following four conditions simultaneously: single-field, canonical kinetic term, slow-roll, and initially vacuum state.

However, the extraction of the primordial non-Gaussianity may not be so simple, as there are various non-primordial effects that can also generate non-Gaussianity. Any non-linearities can make initially Gaussian perturbations non-Gaussian.

The angular bispectrum, $B_{l_1 l_2 l_3}$, the harmonic transform of the angular three-point function, of the Cosmic Microwave Background (CMB) is often used to measure non-Gaussianity (see, e.g., [2], for a review). Departures from any of the above conditions (single-field, canonical kinetic term, slow-roll, and initial vacuum state) would result in detectable non-Gaussian signals in specific triangle configurations of the bispectrum.

When we consider the effects of various non-primordial sources of non-Gaussianity on the extraction of the primordial signals, we must specify of which primordial non-Gaussianity we study the contamination from the non-primordial sources. Multiple-field models, non-canonical kinetic terms, and initially excited states can produce large signals in the squeezed triangles ($l_1 \ll l_2 \approx l_3$) [3], the equilateral triangles ($l_1 = l_2 = l_3$) [4], and the flattened/folded triangles ($l_1 \approx l_2 \approx l_3/2$) [5, 6], respectively.

Throughout this paper we shall study the contamination of the squeezed triangles, parametrized in the form of the so-called local form of the bispectrum, which results from the primordial curvature perturbation (in comoving gauge) in position space, $\zeta(\mathbf{x})$, given by $\zeta(\mathbf{x}) = \zeta_L(\mathbf{x}) + \frac{3}{5}f_{NL}\zeta_L^2(\mathbf{x})$, where ζ_L is a Gaussian perturbation, and f_{NL} characterizes the amplitude of the local-type non-Gaussianity. Our sign convention is such that the temperature anisotropy in the Sachs-Wolfe limit at the first-order in perturbations is given by $\Delta T^{(1)}/T = (1/5)\zeta^{(1)}$. The simplest class of inflation models satisfying all of the four conditions (single-field, canonical kinetic term, slow-roll, and initial vacuum state) produce very small non-Gaussian signals: $f_{NL} \sim 10^{-2}$ at the horizon crossing during inflation [7, 8], whereas the best limit from the WMAP 5-year data with the optimal bispectrum estimator is $f_{NL} = 38 \pm 21$ (68% CL) [9]. How much would non-primordial contributions account for the measured value of f_{NL} ?

The CMB bispectrum from the local-type primordial non-Gaussianity with the linear radiative transfer has been given in [10], and that arising from non-linearity in gravity has been considered in [11]; however, non-linearities exist also in the perturbations in the photon-baryon fluid, i.e., non-linearities in the Boltzmann equation [12, 13, 14].

In this paper we calculate the CMB bispectrum, taking into account the second-order perturbations in the Boltzmann equation. We shall include the second-order terms that are products of the first-order perturbations, and ignore the intrinsically second-order terms (some of them have been considered in [15, 16, 17]), or the effects of the perturbed recombination [18, 19, 20]. The calculations that also include the intrinsically

second-order terms and the perturbed recombination will be presented elsewhere.

2. CMB Bispectrum From Second-order Perturbations

2.1. Definitions

We expand the temperature fluctuation into the linear (first-order) part and the second-order part as

$$\frac{\Delta T(\hat{\mathbf{n}})}{T} = \frac{\Delta T^{(1)}(\hat{\mathbf{n}})}{T} + \frac{\Delta T^{(2)}(\hat{\mathbf{n}})}{T} + \dots \quad (1)$$

The spherical harmonic coefficients of temperature anisotropy, $a_{lm} = T^{-1} \int d^2\hat{\mathbf{n}} Y_{lm}^*(\hat{\mathbf{n}}) \Delta T(\hat{\mathbf{n}})$, are therefore expanded as

$$a_{lm} = a_{lm}^{(1)} + a_{lm}^{(2)} + \dots \quad (2)$$

How do we calculate the second-order part, $a_{lm}^{(2)}$? This can be calculated by expanding the Boltzmann equation up to the second order in perturbations [12].

To expand the Boltzmann equation up to the second order in perturbations, we first expand the distribution function,

$$f(\mathbf{x}, p, \hat{\mathbf{n}}, \eta) = 2 \left[\exp \left\{ \frac{p}{T(\eta) e^{\Theta(\mathbf{x}, \hat{\mathbf{n}}, \eta)}} \right\} - 1 \right]^{-1}, \quad (3)$$

up to the second order in perturbations: $\Theta = \Theta^{(1)} + \Theta^{(2)}/2 + \dots$, and accordingly $f = f^{(0)} + f^{(1)} + f^{(2)}/2 + \dots$

We compute the fractional perturbation in photon's energy density at the i -th order in perturbations, $\Delta^{(i)}$, by multiplying $f^{(i)}$ by p , and integrating over $p^2 dp$:

$$\Delta^{(i)} \equiv \frac{\int dp p^3 f^{(i)}}{\int dp p^3 f^{(0)}}. \quad (4)$$

At the linear order, we recover the usual relation between the linear fractional temperature fluctuation, $\Theta^{(1)} = \Delta T^{(1)}/T$, and the linear fractional energy density perturbation, $\Delta^{(1)} = \delta\rho_\gamma^{(1)}/\rho_\gamma$, i.e., $\Delta^{(1)} = 4\Theta^{(1)}$.

At the second order we have

$$\Delta^{(2)} = 4\Theta^{(2)} + 16[\Theta^{(1)}]^2, \quad (5)$$

which is related to the second-order temperature fluctuation as

$$\begin{aligned} \frac{\Delta T^{(2)}}{T} &= \frac{1}{8} (\Delta^{(2)} - \langle \Delta^{(2)} \rangle) - \frac{3}{2} ([\Theta^{(1)}]^2 - \langle [\Theta^{(1)}]^2 \rangle) \\ &= \frac{1}{2} (\Theta^{(2)} - \langle \Theta^{(2)} \rangle + [\Theta^{(1)}]^2 - \langle [\Theta^{(1)}]^2 \rangle), \end{aligned} \quad (6)$$

where we have subtracted the average of the temperature fluctuation so that the average of $\Delta T^{(2)}/T$ vanishes.

We compute $a_{lm}^{(2)}$ from $\Delta T^{(2)}/T$ using

$$\begin{aligned} a_{lm}^{(2)} &= \int d^2\hat{\mathbf{n}} Y_{lm}^*(\hat{\mathbf{n}}) \frac{\Delta T^{(2)}}{T} \\ &= \tilde{a}_{lm}^{(2)} - \frac{3}{2} \sum_{l'm'} \sum_{l''m''} (-1)^m \mathcal{G}_{l'l''}^{-mm'm''} (a_{l'm'}^{(1)} a_{l''m''}^{(1)} - \langle a_{l'm'}^{(1)} a_{l''m''}^{(1)} \rangle), \end{aligned} \quad (7)$$

where we define

$$\tilde{a}_{lm}^{(2)} \equiv \frac{1}{8} \int d^2\hat{\mathbf{n}} Y_{lm}^*(\hat{\mathbf{n}}) (\Delta^{(2)}(\hat{\mathbf{n}}) - \langle \Delta^{(2)}(\hat{\mathbf{n}}) \rangle), \quad (8)$$

$$\begin{aligned} \mathcal{G}_{l_1 l_2 l_3}^{m_1 m_2 m_3} &\equiv \int d^2\hat{\mathbf{n}} Y_{l_1 m_1}(\hat{\mathbf{n}}) Y_{l_2 m_2}(\hat{\mathbf{n}}) Y_{l_3 m_3}(\hat{\mathbf{n}}) \\ &= \sqrt{\frac{(2l_1+1)(2l_2+1)(2l_3+1)}{4\pi}} \begin{pmatrix} l_1 & l_2 & l_3 \\ 0 & 0 & 0 \end{pmatrix} \begin{pmatrix} l_1 & l_2 & l_3 \\ m_1 & m_2 & m_3 \end{pmatrix}. \end{aligned} \quad (9)$$

Here the matrix is the Wigner $3j$ symbol.

The CMB angular-averaged bispectrum, $B_{l_1 l_2 l_3}$, is related to the ensemble average of $a_{l_1 m_1} a_{l_2 m_2} a_{l_3 m_3}$ as

$$B_{l_1 l_2 l_3} \equiv \sum_{\text{all } m} \begin{pmatrix} l_1 & l_2 & l_3 \\ m_1 & m_2 & m_3 \end{pmatrix} \langle a_{l_1 m_1} a_{l_2 m_2} a_{l_3 m_3} \rangle. \quad (10)$$

This definition guarantees rotational invariance for the bispectrum, and the Wigner $3j$ symbol ensures that the bispectrum must satisfy triangle conditions: $|l_i - l_j| \leq l_k \leq l_i + l_j$ for all permutations of indices, and selection rules: $m_1 + m_2 + m_3 = 0$.

The ensemble average is given by

$$\begin{aligned} \langle a_{l_1 m_1} a_{l_2 m_2} a_{l_3 m_3} \rangle &= \langle a_{l_1 m_1}^{(1)} a_{l_2 m_2}^{(1)} a_{l_3 m_3}^{(2)} \rangle + \text{cyclic} \\ &= \langle a_{l_1 m_1}^{(1)} a_{l_2 m_2}^{(1)} \tilde{a}_{l_3 m_3}^{(2)} \rangle - \frac{3}{2} \sum_{l'_3 m'_3} \sum_{l''_3 m''_3} (-1)^{m_3} \mathcal{G}_{l_3 l'_3 l''_3}^{-m_3 m'_3 m''_3} \\ &\quad \times (\langle a_{l_1 m_1}^{(1)} a_{l_2 m_2}^{(1)} a_{l'_3 m'_3}^{(1)} a_{l''_3 m''_3}^{(1)} \rangle - \langle a_{l_1 m_1}^{(1)} a_{l_2 m_2}^{(1)} \rangle \langle a_{l'_3 m'_3}^{(1)} a_{l''_3 m''_3}^{(1)} \rangle) + \text{cyclic}, \end{aligned} \quad (11)$$

where *cyclic* means that we have to sum the cyclic permutations of Eq. (11) for indices $(1, 2, 3) \rightarrow (3, 1, 2) \rightarrow (2, 3, 1)$.

As we assume that $a_{lm}^{(1)}$'s are Gaussian random variables, the four-point function of $a_{lm}^{(1)}$'s in Eq. (11) is given by the sum of products of all possible pairs. Each pair gives the angular power spectrum, C_l :

$$\langle a_{lm}^{(1)} a_{l'm'}^{(1)} \rangle = (-1)^m C_l \delta_{ll'} \delta_{-mm'}. \quad (12)$$

We obtain

$$\begin{aligned} \langle a_{l_1 m_1}^{(1)} a_{l_2 m_2}^{(1)} a_{l'_3 m'_3}^{(1)} a_{l''_3 m''_3}^{(1)} \rangle &- \langle a_{l_1 m_1}^{(1)} a_{l_2 m_2}^{(1)} \rangle \langle a_{l'_3 m'_3}^{(1)} a_{l''_3 m''_3}^{(1)} \rangle \\ &= (-1)^{m_1+m_2} C_{l_1} C_{l_2} [\delta_{l_1 l'_3} \delta_{-m_1 m'_3} \delta_{l_2 l''_3} \delta_{-m_2 m''_3} + (1 \leftrightarrow 2)]. \end{aligned} \quad (13)$$

Substituting the right hand side of equation (13) for the second term of equation (11), and using $l_1 + l_2 + l_3 = \text{even}$, we obtain the angular averaged bispectrum,

$$B_{l_1 l_2 l_3} = \tilde{B}_{l_1 l_2 l_3} - 3I_{l_1 l_2 l_3} (C_{l_1} C_{l_2} + \text{cyclic}), \quad (14)$$

where we have defined the quantities,

$$I_{l_1 l_2 l_3} \equiv \sqrt{\frac{(2l_1 + 1)(2l_2 + 1)(2l_3 + 1)}{4\pi}} \begin{pmatrix} l_1 & l_2 & l_3 \\ 0 & 0 & 0 \end{pmatrix}, \quad (15)$$

and

$$\tilde{B}_{l_1 l_2 l_3} = \sum_{\text{all } m} \begin{pmatrix} l_1 & l_2 & l_3 \\ m_1 & m_2 & m_3 \end{pmatrix} \langle a_{l_1 m_1}^{(1)} a_{l_2 m_2}^{(1)} \tilde{a}_{l_3 m_3}^{(2)} \rangle + \text{cyclic}. \quad (16)$$

2.2. Angular averaged bispectrum from second-order perturbations

The Boltzmann equation governs the evolution of $\Delta^{(1)}(k, \mu, \eta)$ and $\Delta^{(2)}(\mathbf{k}, \hat{\mathbf{n}}, \eta)$, where $\mu = \hat{k} \cdot \hat{n}$ and \mathbf{n} is the direction of propagation of photons. Note that for the linear perturbation there is azimuthal symmetry such that $\Delta^{(1)}$ depends only on the angle between \mathbf{k} and \mathbf{n} ; however, for the second-order perturbation there is no such symmetry. The Boltzmann equations in Fourier space are given by

$$\Delta^{(1)'} + ik\mu\Delta^{(1)} - \tau'\Delta^{(1)} = S^{(1)}(k, \mu, \eta), \quad (17)$$

$$\Delta^{(2)'} + ik\mu\Delta^{(2)} - \tau'\Delta^{(2)} = S^{(2)}(\mathbf{k}, \hat{\mathbf{n}}, \eta), \quad (18)$$

where the primes denote derivatives with respect to the conformal time $\partial/\partial\eta$, $S^{(1)}$ and $S^{(2)}$ are the source functions at the first and the second orders, respectively, and τ' is the differential optical depth which is defined by using the mean electron number density, \bar{n}_e , the Thomson scattering cross-section, σ_T , and the scale factor, a , as

$$\tau' = -\bar{n}_e \sigma_T a. \quad (19)$$

We expand the angular dependence of $\Delta^{(i)}$ as

$$\Delta_{lm}^{(i)}(\mathbf{k}, \eta) = i^l \sqrt{\frac{2l+1}{4\pi}} \int d^2\hat{\mathbf{n}} Y_{lm}^*(\hat{\mathbf{n}}) \Delta^{(i)}(\mathbf{k}, \hat{\mathbf{n}}, \eta), \quad (20)$$

and that of the source terms as

$$S_{lm}^{(i)}(\mathbf{k}, \eta) = i^l \sqrt{\frac{2l+1}{4\pi}} \int d^2\hat{\mathbf{n}} Y_{lm}^*(\hat{\mathbf{n}}) S^{(i)}(\mathbf{k}, \hat{\mathbf{n}}, \eta), \quad (21)$$

where $i = 1, 2$.

The source functions relate the observed a_{lm} 's to the primordial curvature perturbations in comoving gauge, $\zeta(\mathbf{k})$. The relations contain the linear radiation transfer function, $g_l(k)$, and the second-order radiation transfer function, $F_{lm}^{l'm'}(k)$, and are given by

$$a_{lm}^{(1)} = 4\pi(-i)^l \int \frac{d^3k}{(2\pi)^3} g_l(k) Y_{lm}^*(\hat{\mathbf{k}}) \zeta(\mathbf{k}), \quad (22)$$

$$\begin{aligned} \tilde{a}_{lm}^{(2)} &= \frac{4\pi}{8}(-i)^l \int \frac{d^3k}{(2\pi)^3} \int \frac{d^3k'}{(2\pi)^3} \int d^3k'' \delta^3(\mathbf{k}' + \mathbf{k}'' - \mathbf{k}) \\ &\quad \times \sum_{l'm'} F_{lm}^{l'm'}(\mathbf{k}', \mathbf{k}'', \mathbf{k}) Y_{l'm'}^*(\hat{\mathbf{k}}) \zeta(\mathbf{k}') \zeta(\mathbf{k}''). \end{aligned} \quad (23)$$

The linear transfer function is given by

$$g_l(k) = \int_0^{\eta_0} d\eta e^{-\tau} \left[S_{00}^{(1)}(k, \eta) + S_{10}^{(1)}(k, \eta) \frac{d}{du} + S_{20}^{(1)}(k, \eta) \left(\frac{3}{2} \frac{d^2}{du^2} + \frac{1}{2} \right) \right] j_l(u), \quad (24)$$

where $u \equiv k(\eta_0 - \eta)$ and $S_{lm}^{(1)}$ is the standard linear source function (e.g., [22]):

$$S_{00}^{(1)}(k, \eta) = 4\Psi^{(1)'}(k, \eta) - \tau' \Delta_0^{(1)}(k, \eta), \quad (25)$$

$$S_{10}^{(1)}(k, \eta) = 4k\Phi^{(1)}(k, \eta) - 4\tau'v_0^{(1)}(k, \eta), \quad (26)$$

$$S_{20}^{(1)}(k, \eta) = \frac{\tau'}{2} \Delta_2^{(1)}(k, \eta), \quad (27)$$

where $\Phi^{(1)}(k, \eta)$ and $\Psi^{(1)}(k, \eta)$ are the metric perturbations at the linear order in the longitudinal gauge:

$$ds^2 = a^2(\eta) [-(1 + 2\Phi^{(1)})d\eta^2 + (1 - 2\Psi^{(1)})\delta_{ij}dx^i dx^j], \quad (28)$$

and $\Delta_0^{(1)}(k, \eta)$, $\Delta_1^{(1)}(k, \eta)$, and $\Delta_2^{(1)}(k, \eta)$ are the coefficients of the expansion in Legendre polynomials of $\Delta^{(1)}(k, \mu, \eta)$, and $\Delta_l^{(1)}(k, \eta)$ is related to $\Delta_{lm}^{(1)}$ (Eq. (20)) via $\Delta_{lm}^{(1)} = (-i)^{-l}(2l+1)\Delta_l^{(1)}\delta_{m0}$. The first-order velocity perturbation, $v_0^{(1)}(k, \eta)$, is the irrotational part of the baryon velocity defined by $\mathbf{v}(\mathbf{k}) = -iv_0(k)\hat{\mathbf{k}}$.

The new piece, the second-order transfer function, is the line-of-sight integral of the second-order source terms in the Boltzmann equation:

$$\begin{aligned} F_{lm}^{\prime m'}(\mathbf{k}', \mathbf{k}'', \mathbf{k}) &= i^l \sum_{\lambda\mu} (-1)^m (-i)^{\lambda-l'} \mathcal{G}_{l\lambda}^{-mm'\mu} \sqrt{\frac{4\pi}{2\lambda+1}} \\ &\times \int_0^{\eta_0} d\eta e^{-\tau} \mathcal{S}_{\lambda\mu}^{(2)}(\mathbf{k}', \mathbf{k}'', \mathbf{k}, \eta) j_{l'}[k(\eta - \eta_0)]. \end{aligned} \quad (29)$$

Here, we have introduced a new function, $\mathcal{S}_{lm}^{(2)}(\mathbf{k}', \mathbf{k}'', \mathbf{k}, \eta)$, which is defined by the following equation:

$$S_{lm}^{(2)}(\mathbf{k}, \eta) = \int \frac{d^3 k'}{(2\pi)^3} \int d^3 k'' \delta^3(\mathbf{k}' + \mathbf{k}'' - \mathbf{k}) \mathcal{S}_{lm}^{(2)}(\mathbf{k}', \mathbf{k}'', \mathbf{k}, \eta) \zeta(\mathbf{k}') \zeta(\mathbf{k}''). \quad (30)$$

Basically, $\mathcal{S}_{lm}^{(2)}(\mathbf{k}', \mathbf{k}'', \mathbf{k}, \eta)$ is the second-order source function divided by $\zeta(\mathbf{k}')\zeta(\mathbf{k}'')$.

The explicit expression for $S_{lm}^{(2)}(\mathbf{k}, \eta)$ in terms of perturbation variables is given by Ref. [12]. Using equation (22) and (23), we calculate the first term in Eq. (14), $\tilde{B}_{l_1 l_2 l_3}$, as follows:

$$\begin{aligned} \langle a_{l_1 m_1}^{(1)} a_{l_2 m_2}^{(1)} \tilde{a}_{l_3 m_3}^{(2)} \rangle &= \frac{(-i)^{l_1+l_2+l_3}}{(2\pi)^3} \sum_{L_3 M_3} \prod_i \int d^3 k_i \delta^3(\sum_i \mathbf{k}_i) Y_{l_1 m_1}^*(\hat{\mathbf{k}}_1) Y_{l_2 m_2}^*(\hat{\mathbf{k}}_2) Y_{L_3 M_3}^*(\hat{\mathbf{k}}_3) \\ &\times g_{l_1}(k_1) g_{l_2}(k_2) P_\zeta(k_1) P_\zeta(k_2) \{ F_{l_3 m_3}^{L_3 M_3}(\mathbf{k}_1, \mathbf{k}_2, \mathbf{k}_3) + F_{l_3 m_3}^{L_3 M_3}(\mathbf{k}_2, \mathbf{k}_1, \mathbf{k}_3) \}, \end{aligned} \quad (31)$$

where $P_\zeta(k)$ is the power spectrum of ζ given by the usual definition:

$$\langle \zeta(\mathbf{k}_1) \rangle = 0, \quad \langle \zeta(\mathbf{k}_1) \zeta(\mathbf{k}_2) \rangle = (2\pi)^3 \delta^3(\mathbf{k}_1 + \mathbf{k}_2) P_\zeta(k_1). \quad (32)$$

In order to perform the integral over angles, $\hat{\mathbf{k}}$, we expand the three-dimensional δ -function using Rayleigh's formula,

$$\begin{aligned} \delta^3(\mathbf{k}_1 + \mathbf{k}_2 + \mathbf{k}_3) &= 8 \sum_{\text{all } l' m'} i^{l'_1+l'_2+l'_3} \mathcal{G}_{l'_1 l'_2 l'_3}^{m'_1 m'_2 m'_3} Y_{l'_1 m'_1}(\hat{\mathbf{k}}_1) Y_{l'_2 m'_2}(\hat{\mathbf{k}}_2) Y_{l'_3 m'_3}(\hat{\mathbf{k}}_3) \\ &\times \int dr r^2 j_{l'_1}(r k_1) j_{l'_2}(r k_2) j_{l'_3}(r k_3), \end{aligned} \quad (33)$$

and also expand the angular dependence of $\mathcal{S}_{lm}^{(2)}(\mathbf{k}_1, \mathbf{k}_2, \mathbf{k}_3, \eta)$ by introducing the transformed source function, $\mathcal{S}_{\lambda_1 \lambda_2 \lambda_3}^{\mu_1 \mu_2 \mu_3}(k_1, k_2, k_3, \eta)$, as

$$\begin{aligned} \mathcal{S}_{\lambda_3 \mu_3}^{(2)}(\mathbf{k}_1, \mathbf{k}_2, \mathbf{k}_3, \eta) &= \sum_{\lambda_1, \mu_1} \sum_{\lambda_2, \mu_2} (-i)^{\lambda_1 + \lambda_2} \sqrt{\frac{4\pi}{2\lambda_1 + 1}} \sqrt{\frac{4\pi}{2\lambda_2 + 1}} \\ &\times \mathcal{S}_{\lambda_1 \lambda_2 \lambda_3}^{\mu_1 \mu_2 \mu_3}(k_1, k_2, k_3, \eta) Y_{\lambda_1 \mu_1}(\hat{\mathbf{k}}_1) Y_{\lambda_2 \mu_2}(\hat{\mathbf{k}}_2). \end{aligned} \quad (34)$$

This result shows that $\mathcal{S}_{\lambda_3 \mu_3}^{(2)}(\mathbf{k}_1, \mathbf{k}_2, \mathbf{k}_3, \eta) = \mathcal{S}_{\lambda_3 \mu_3}^{(2)}(\mathbf{k}_1, \mathbf{k}_2, k_3, \eta)$, and thus $F_{lm}^{l' m'}(\mathbf{k}_1, \mathbf{k}_2, k_3)$ follows (see Eq. (29)).

Now we can perform the angular integration of Eq. (31) to obtain

$$\begin{aligned} \tilde{B}_{l_1 l_2 l_3} &= \frac{4}{\pi^2} (-i)^{l_1 + l_2 + l_3} \sum_{\text{all } m} \sum_{\text{all } l' m'} \sum_{\text{all } \lambda \mu} \sqrt{\frac{4\pi}{(2\lambda_1 + 1)(2\lambda_2 + 1)(2\lambda_3 + 1)}} i^{l'_1 + l'_2 + l'_3 - \lambda_1 - \lambda_2 - \lambda_3} \\ &\times \begin{pmatrix} l_1 & l_2 & l_3 \\ m_1 & m_2 & m_3 \end{pmatrix} \mathcal{G}_{l'_1 l'_2 l'_3}^{m'_1 m'_2 m'_3} \mathcal{G}_{l'_1 l_1 \lambda_1}^{m'_1 - m_1 \mu_1} \mathcal{G}_{l'_2 l_2 \lambda_2}^{m'_2 - m_2 \mu_2} \mathcal{G}_{l'_3 l_3 \lambda_3}^{m'_3 - m_3 \mu_3} \\ &\times \prod_{i=1}^3 \int k_i^2 dk_i \int dr r^2 j_{l'_1}(r k_1) j_{l'_2}(r k_2) j_{l'_3}(r k_3) g_{l_1}(k_1) g_{l_2}(k_2) P_\zeta(k_1) P_\zeta(k_2) \\ &\times i^{l_3 + l'_3} \int d\eta e^{-\tau} \{ \mathcal{S}_{\lambda_1 \lambda_2 \lambda_3}^{\mu_1 \mu_2 \mu_3}(k_1, k_2, k_3, \eta) + \mathcal{S}_{\lambda_2 \lambda_1 \lambda_3}^{\mu_2 \mu_1 \mu_3}(k_2, k_1, k_3, \eta) \} j_{l'_3}[k_3(\eta - \eta_0)] \\ &+ \text{cyclic}, \end{aligned} \quad (35)$$

where we have used the following relation of the Wigner $9j$ symbol,

$$\begin{aligned} (-1)^{l'_1 + l'_2 + l'_3} \sum_{\text{all } m m'} \begin{pmatrix} l_1 & l_2 & l_3 \\ m_1 & m_2 & m_3 \end{pmatrix} \mathcal{G}_{l'_1 l'_2 l'_3}^{m'_1 m'_2 m'_3} \mathcal{G}_{l'_1 l_1 \lambda_1}^{m'_1 - m_1 \mu_1} \mathcal{G}_{l'_2 l_2 \lambda_2}^{m'_2 - m_2 \mu_2} \mathcal{G}_{l'_3 l_3 \lambda_3}^{m'_3 - m_3 \mu_3} \\ = (-1)^R I_{l'_1 l'_2 l'_3} I_{l_1 l'_1 \lambda_1} I_{l_2 l'_2 \lambda_2} I_{l_3 l'_3 \lambda_3} \left\{ \begin{matrix} l_1 & l_2 & l_3 \\ l'_1 & l'_2 & l'_3 \\ \lambda_1 & \lambda_2 & \lambda_3 \end{matrix} \right\} \begin{pmatrix} \lambda_1 & \lambda_2 & \lambda_3 \\ \mu_1 & \mu_2 & \mu_3 \end{pmatrix}, \end{aligned} \quad (36)$$

where $R \equiv l_1 + l_2 + l_3 + l'_1 + l'_2 + l'_3 + \lambda_1 + \lambda_2 + \lambda_3$. The Wigner $9j$ symbols have the permutation symmetry:

$$\begin{aligned} (-1)^R \left\{ \begin{matrix} l_1 & l_2 & l_3 \\ l'_1 & l'_2 & l'_3 \\ \lambda_1 & \lambda_2 & \lambda_3 \end{matrix} \right\} &= \left\{ \begin{matrix} l_2 & l_1 & l_3 \\ l'_2 & l'_1 & l'_3 \\ \lambda_2 & \lambda_1 & \lambda_3 \end{matrix} \right\} = \left\{ \begin{matrix} l_1 & l_3 & l_2 \\ l'_1 & l'_3 & l'_2 \\ \lambda_1 & \lambda_3 & \lambda_2 \end{matrix} \right\} \\ &= \left\{ \begin{matrix} l'_1 & l'_2 & l'_3 \\ l_1 & l_2 & l_3 \\ \lambda_1 & \lambda_2 & \lambda_3 \end{matrix} \right\} = \left\{ \begin{matrix} l_1 & l_2 & l_3 \\ \lambda_1 & \lambda_2 & \lambda_3 \\ l'_1 & l'_2 & l'_3 \end{matrix} \right\}, \end{aligned} \quad (37)$$

and the coefficients $I_{l'_1 l'_2 l'_3}$, $I_{l'_1 l'_1 \lambda_1}$, $I_{l'_2 l'_2 \lambda_2}$, and $I_{l'_3 l'_3 \lambda_3}$, ensure $l'_1 + l'_2 + l'_3 = \text{even}$, $l_1 + l'_1 + \lambda_1 = \text{even}$, $l_2 + l'_2 + \lambda_2 = \text{even}$, and $l_3 + l'_3 + \lambda_3 = \text{even}$, respectively, which gives $R = \text{even}$. Hence the Wigner $9j$ coefficients are invariant under the permutations.

Finally, we obtain the angular averaged bispectrum,

$$\begin{aligned} \tilde{B}_{l_1 l_2 l_3} = & \frac{4}{\pi^2} \sum_{\text{all } l' \lambda} \sqrt{\frac{4\pi}{(2\lambda_1 + 1)(2\lambda_2 + 1)(2\lambda_3 + 1)}} i^{l_3 - l'_3 + R} I_{l'_1 l'_2 l'_3} I_{l'_1 l'_1 \lambda_1} I_{l'_2 l'_2 \lambda_2} I_{l'_3 l'_3 \lambda_3} \left\{ \begin{array}{ccc} l_1 & l_2 & l_3 \\ l'_1 & l'_2 & l'_3 \\ \lambda_1 & \lambda_2 & \lambda_3 \end{array} \right\} \\ & \times \int dr r^2 \prod_{i=1}^2 \int dk_i k_i^2 P_\zeta(k_i) g_{l_i}(k_i) j_{l'_i}(rk_i) \int dk_3 k_3^2 j_{l'_3}(rk_3) \\ & \times \int dr' e^{-\tau(r')} j_{l'_3}(r'k_3) \mathcal{S}_{\lambda_1 \lambda_2 \lambda_3}(k_1, k_2, k_3, r') + \text{perm}, \end{aligned} \quad (38)$$

where $r' \equiv \eta_0 - \eta$ and we have used the relation of the spherical Bessel function, $j_l(-x) = (-1)^l j_l(x)$, and have defined the ‘‘angular-averaged source function,’’

$$\mathcal{S}_{\lambda_1 \lambda_2 \lambda_3}(k_1, k_2, k_3, r) \equiv \sum_{\text{all } \mu} \left(\begin{array}{ccc} \lambda_1 & \lambda_2 & \lambda_3 \\ \mu_1 & \mu_2 & \mu_3 \end{array} \right) \mathcal{S}_{\lambda_1 \lambda_2 \lambda_3}^{\mu_1 \mu_2 \mu_3}(k_1, k_2, k_3, r). \quad (39)$$

Note that *cyclic* terms in Eq. (35) have become *perm* (permutations) because of invariance of the Wigner $9j$ coefficients under the permutations.

The final analytic formula (38) we have obtained is a general formula which can be applied to any second-order perturbations. The information about the specific second-order terms is contained in the angular-averaged source term, $\mathcal{S}_{\lambda_1 \lambda_2 \lambda_3}$ (see Eqs. (39) and (34) for the definition).

For products of the first-order terms, we shall show later that $\mathcal{S}_{\lambda_1 \lambda_2 \lambda_3}(k_1, k_2, k_3, \eta)$ does not depend on k_3 , i.e., $\mathcal{S}_{\lambda_1 \lambda_2 \lambda_3}(k_1, k_2, k_3, \eta) = \mathcal{S}_{\lambda_1 \lambda_2 \lambda_3}(k_1, k_2, \eta)$. This property enables us to integrate Eq. (38) over k_3 . We obtain

$$\begin{aligned} \tilde{B}_{l_1 l_2 l_3} = & \frac{2}{\pi} \sum_{\text{all } l' \lambda} \sqrt{\frac{4\pi}{(2\lambda_1 + 1)(2\lambda_2 + 1)(2\lambda_3 + 1)}} i^{l_3 - l'_3 + R} I_{l'_1 l'_2 l'_3} I_{l'_1 l'_1 \lambda_1} I_{l'_2 l'_2 \lambda_2} I_{l'_3 l'_3 \lambda_3} \left\{ \begin{array}{ccc} l_1 & l_2 & l_3 \\ l'_1 & l'_2 & l'_3 \\ \lambda_1 & \lambda_2 & \lambda_3 \end{array} \right\} \\ & \times \int dr e^{-\tau} \prod_{i=1}^2 \int dk_i k_i^2 P_\zeta(k_i) j_{l'_i}(rk_i) g_{l_i}(k_i) \mathcal{S}_{\lambda_1 \lambda_2 \lambda_3}(k_1, k_2, r) + \text{perm}, \end{aligned} \quad (40)$$

where $r \equiv \eta_0 - \eta$, $R = l_1 + l_2 + l_3 + l'_1 + l'_2 + l'_3 + \lambda_1 + \lambda_2 + \lambda_3$, and we have used

$$\int dk_3 k_3^2 j_{l'_3}(rk_3) j_{l'_3}(r'k_3) = \frac{\pi}{2r^2} \delta(r - r'). \quad (41)$$

Finally, by adding the remaining term in the full bispectrum, Eq. (14), we obtain

$$\begin{aligned} B_{l_1 l_2 l_3} = & \frac{2}{\pi} \sum_{\text{all } l' \lambda} \sqrt{\frac{4\pi}{(2\lambda_1 + 1)(2\lambda_2 + 1)(2\lambda_3 + 1)}} i^{l_3 - l'_3 + R} I_{l'_1 l'_2 l'_3} I_{l'_1 l'_1 \lambda_1} I_{l'_2 l'_2 \lambda_2} I_{l'_3 l'_3 \lambda_3} \left\{ \begin{array}{ccc} l_1 & l_2 & l_3 \\ l'_1 & l'_2 & l'_3 \\ \lambda_1 & \lambda_2 & \lambda_3 \end{array} \right\} \\ & \times \int dr e^{-\tau} \prod_{i=1}^2 \int dk_i k_i^2 P_\zeta(k_i) j_{l'_i}(rk_i) g_{l_i}(k_i) \mathcal{S}_{\lambda_1 \lambda_2 \lambda_3}(k_1, k_2, r) - \frac{3}{2} I_{l_1 l_2 l_3} C_{l_1} C_{l_2} + \text{perm}. \end{aligned} \quad (42)$$

The remaining task is to calculate the angular-averaged source term, $\mathcal{S}_{\lambda_1\lambda_2\lambda_3}(k_1, k_2, \eta)$, which will be given in the next section.

3. Second-order bispectrum from products of the first-order terms

3.1. Source Term

The explicit expressions for the second-order source term in Fourier space are given by Eq. (5.19) of [12]. We will choose the coordinate system such that $\hat{\mathbf{e}}_3 = \hat{\mathbf{k}}$ in their expressions, i.e., $\hat{\mathbf{e}}_1 \perp \hat{\mathbf{k}}$, $\hat{\mathbf{e}}_2 \perp \hat{\mathbf{k}}$, and $\hat{\mathbf{e}}_1 \perp \hat{\mathbf{e}}_2$, and adopt the following metric convention:

$$ds^2 = a^2(\eta) \left[-e^{2\Phi} d\eta^2 + 2\omega_i dx^i d\eta + (e^{-2\Psi} \delta_{ij} + \chi_{ij}) dx^i dx^j \right], \quad (43)$$

where $\Phi = \Phi^{(1)} + \Phi^{(2)}/2$, $\Psi = \Psi^{(1)} + \Psi^{(2)}/2$, and the shift vector, ω_i , and the transverse and traceless tensor metric perturbation, χ_{ij} , are already at the second order. Note that the first-order part of this metric is equivalent to Eq. (28). The second-order source term is [12, 21] (also see [14]) ‡

$$\begin{aligned} S_{lm}(\mathbf{k}, \eta) = & (4\Psi^{(2)'} - \tau' \Delta_{00}^{(2)}) \delta_{l0} \delta_{m0} + 4k\Phi^{(2)} \delta_{l1} \delta_{m0} - 8\omega'_m \delta_{l1} - 4\tau' v_m^{(2)} \delta_{l1} - \frac{\tau'}{10} \Delta_{lm}^{(2)} \delta_{l2} - 4\chi'_m \delta_{l2} \\ & + \int \frac{d^3 k_1}{(2\pi)^3} \left\{ -2\tau' [(\delta_e^{(1)} + \Phi^{(1)})(\mathbf{k}_1) \Delta_0^{(1)}(\mathbf{k}_2) + 2iv_0^{(1)}(\mathbf{k}_1) \Delta_1^{(1)}(\mathbf{k}_2)] \delta_{l0} \delta_{m0} \right. \\ & + 4k\Phi^{(1)}(\mathbf{k}_1) \Phi^{(1)}(\mathbf{k}_2) \delta_{l1} \delta_{m0} + \tau' [(\delta_e^{(1)} + \Phi^{(1)})(\mathbf{k}_1) \Delta_2^{(1)}(\mathbf{k}_2) + 2iv_0^{(1)}(\mathbf{k}_1) \Delta_1^{(1)}(\mathbf{k}_2)] \delta_{l2} \delta_{m0} \\ & \left. + [8\Psi^{(1)'}(\mathbf{k}_1) + 2\tau'(\delta_e^{(1)} + \Phi^{(1)})(\mathbf{k}_1)] \Delta_{l0}^{(1)}(\mathbf{k}_2) \delta_{m0} \right\} \\ & - \int \frac{d^3 k_1}{(2\pi)^3} \hat{\mathbf{k}}_1 \cdot \hat{\mathbf{k}}_2 \left\{ 2\tau' v_0^{(1)}(\mathbf{k}_1) v_0^{(1)}(\mathbf{k}_2) \delta_{l0} - i(-i)^{-l} (2l+1) k_1 (\Psi^{(1)} + \Phi^{(1)})(\mathbf{k}_1) \right. \\ & \left. \times \sum_L (2L+1) \Delta_L^{(1)}(\mathbf{k}_2) \int d\mu P_L(\mu) \frac{\partial P_L(\mu)}{\partial \mu} \right\} \delta_{m0} \\ & - 2 \left[4\Psi^{(1)} \nabla \Phi^{(1)} + 4\tau' (\delta_e^{(1)} + \Phi^{(1)}) \mathbf{v} + 3\tau' \Delta_0^{(1)} \mathbf{v} - \tau' \Delta_2^{(1)} \mathbf{v} \right]_m \delta_{l1} \\ & + i(-i)^{-l} (-1)^{-m} (2l+1) \sum_{l''} \sum_{m'=-1}^1 (2l''+1) \begin{pmatrix} l'' & 1 & l \\ 0 & 0 & 0 \end{pmatrix} \begin{pmatrix} l'' & 1 & l \\ 0 & m' & -m \end{pmatrix} \\ & \times \left[8\Delta_{l''}^{(1)} \nabla \Phi^{(1)} + 2(\Psi^{(1)} + \Phi^{(1)}) \nabla \Delta_{l''}^{(1)} + 2\tau' \Delta_{l''}^{(1)} \mathbf{v} + 5\delta_{l''2} \tau' \Delta_2^{(1)} \mathbf{v} \right]_{m'} \\ & + 14\tau' (-i)^{-l} (-1)^{-m} (2l+1) \sum_{m', m''=-1}^1 \begin{pmatrix} 1 & 1 & l \\ 0 & 0 & 0 \end{pmatrix} \begin{pmatrix} 1 & 1 & l \\ m' & m'' & -m \end{pmatrix} \\ & \times \frac{4\pi}{3} \int \frac{d^3 k_1}{(2\pi)^3} v_0^{(1)}(\mathbf{k}_1) v_0^{(1)}(\mathbf{k}_2) Y_{1m'}^*(\hat{\mathbf{k}}_1) Y_{1m''}^*(\hat{\mathbf{k}}_2) \\ & - 2i(-i)^{-l} \sqrt{\frac{3l+1}{4\pi}} \sum_{m', m''=-1}^1 \sum_L (2L+1) \int d^2 \hat{\mathbf{n}} Y_{1m'}(\hat{\mathbf{n}}) Y_{1m''}(\hat{\mathbf{n}}) Y_{lm}^*(\hat{\mathbf{n}}) \frac{\partial P_L(\mu)}{\partial \mu} \\ & \times \left(\frac{4\pi}{3} \right)^2 \int \frac{d^3 k_1}{(2\pi)^3} k_1 (\Psi^{(1)} + \Phi^{(1)})(\mathbf{k}_1) \Delta_L^{(1)}(\mathbf{k}_2) Y_{1m'}^*(\hat{\mathbf{k}}_1) Y_{1m''}^*(\hat{\mathbf{k}}_2), \quad (44) \end{aligned}$$

‡ We have corrected the source term given in Refs. [12, 21] for typos, errors, and some missing terms.

where $\mathbf{k} = \mathbf{k}_1 + \mathbf{k}_2$, and $\mu = \hat{\mathbf{n}} \cdot \hat{\mathbf{k}}$

Here, we have introduced several variables that require explanations. The first-order electron number density perturbation is defined by

$$n_e = \bar{n}_e(1 + \delta_e^{(1)}). \quad (45)$$

The first-order velocity perturbation, $\mathbf{v}^{(1)}(\mathbf{k})$, consists only of the scalar (longitudinal) perturbation:

$$\mathbf{v}^{(1)}(\mathbf{k}) = -iv_0^{(1)}\hat{\mathbf{e}}_3. \quad (46)$$

The second-order velocity perturbation, $\mathbf{v}^{(2)}(\mathbf{k})$, consists of the scalar perturbation, $v_0^{(2)}$, and the vector (transverse) perturbation, $v_m^{(2)}$:

$$\mathbf{v}^{(2)}(\mathbf{k}) = -iv_0^{(2)}\hat{\mathbf{e}}_3 + \sum_{m=\pm 1} v_m^{(2)} \frac{\hat{\mathbf{e}}_2 \mp \hat{\mathbf{e}}_1}{\sqrt{2}}. \quad (47)$$

The second-order shift vector, $\omega(\mathbf{k})$, is decomposed in a similar way:

$$\omega(\mathbf{k}) = \sum_{m=\pm 1} \omega_m \frac{\hat{\mathbf{e}}_2 \mp \hat{\mathbf{e}}_1}{\sqrt{2}}. \quad (48)$$

In the gauge choice of [12], there is no scalar mode in the shift vector. For the tensor metric perturbation, χ_{ij} , we have

$$\chi_{ij} = -\sqrt{\frac{3}{8}} \sum_{m=\pm 2} \chi_m (\hat{\mathbf{e}}_1 \pm i\hat{\mathbf{e}}_2)_i (\hat{\mathbf{e}}_1 \pm i\hat{\mathbf{e}}_2)_j. \quad (49)$$

The quantities, $(f\mathbf{v})_m$ and $(f\nabla g)_m$, are given by

$$(f\mathbf{v})_m(\mathbf{k}) = \sqrt{\frac{4\pi}{3}} \int \frac{d^3k_1}{(2\pi)^3} v_0(\mathbf{k}_1) f(\mathbf{k} - \mathbf{k}_1) Y_{1m}^*(\hat{\mathbf{k}}_1), \quad (50)$$

and

$$(f\nabla g)_m(\mathbf{k}) = -\sqrt{\frac{4\pi}{3}} \int \frac{d^3k_1}{(2\pi)^3} k_1 g(\mathbf{k}_1) f(\mathbf{k} - \mathbf{k}_1) Y_{1m}^*(\hat{\mathbf{k}}_1), \quad (51)$$

respectively.

These perturbation variables of the source term can be split into two parts; the first line of Eq. (44) contains the variables that are intrinsically second-order. (The variables have superscripts (2), and ω_m and χ_m are also intrinsically second-order.) Solving for these terms requires solving the full second-order Boltzmann equations coupled with the Einstein equations.

The other lines contain the terms that are products of two linear variables. Evaluation of these terms is much easier than that of the intrinsically second-order terms, as the first-order variables have already been calculated using the standard linearized Boltzmann code such as CMBFAST [22].

Throughout this paper, we shall evaluate only the products of the first-order perturbations. The intrinsically second-order perturbations are equally important, and

therefore the final results must also include those second-order terms. We shall also neglect the contribution from perturbing the recombination history [18, 19, 20] for now; we shall present the full results elsewhere.

For the products of the first-order perturbations, the source terms, $\mathcal{S}_{\lambda_1\lambda_2\lambda_3}$, are non-zero only for the following four cases (for notational simplicity we shall omit the superscripts (1)):

$$\begin{aligned}
 \mathcal{S}_{000} &= 4i\tau'v_0(k_1)\Delta_1(k_2) + 8\Psi'(k_1)\Delta_0(k_2), \\
 \mathcal{S}_{110} &= \frac{4}{\sqrt{3}}\left\{-5\tau'v_0(k_1)v_0(k_2) + 2k_1(\Psi + \Phi)(k_1) \sum_{L=odd} (2L+1)\Delta_L(k_2)\right\}, \\
 \mathcal{S}_{101} &= 2i\sqrt{3}\left\{\tau'v_0(k_1)(4\delta_e + 4\Phi + 2\Delta_0 - \Delta_2)(k_2) \right. \\
 &\quad \left. + 4k_1\Phi(k_1)(\Delta_0 - \Psi)(k_2) + k_1\Delta_0(k_1)(\Psi + \Phi)(k_2)\right\}, \\
 \mathcal{S}_{112} &= 2\sqrt{\frac{10}{3}}\left\{7\tau'v_0(k_1)v_0(k_2) - k_1(\Psi + \Phi)(k_1) \sum_{L=odd} (2L+1)\Delta_L(k_2)\right\}. \tag{52}
 \end{aligned}$$

From these results we find that $\mathcal{S}_{\lambda_1\lambda_2\lambda_3}$ does not depend on k_3 , i.e., $\mathcal{S}_{\lambda_1\lambda_2\lambda_3} = \mathcal{S}_{\lambda_1\lambda_2\lambda_3}(k_1, k_2, r)$. Note also that $\mathcal{S}_{011}(k_1, k_2, r) = \mathcal{S}_{101}(k_2, k_1, r)$. We have obtained these results by performing the following summation over μ_1, μ_2 , and μ_3 :

$$\begin{aligned}
 \mathcal{S}_{\lambda_1\lambda_2\lambda_3}(k_1, k_2, r) &= \sum_{\text{all}\mu} \begin{pmatrix} \lambda_1 & \lambda_2 & \lambda_3 \\ \mu_1 & \mu_2 & \mu_3 \end{pmatrix} \mathcal{S}_{\lambda_1\lambda_2\lambda_3}^{\mu_1\mu_2\mu_3}(k_1, k_2, r) \\
 &= i^{\lambda_1+\lambda_2} \sqrt{\frac{2\lambda_1+1}{4\pi}} \sqrt{\frac{2\lambda_2+1}{4\pi}} \sum_{\text{all}\mu} \begin{pmatrix} \lambda_1 & \lambda_2 & \lambda_3 \\ \mu_1 & \mu_2 & \mu_3 \end{pmatrix} \\
 &\quad \times \int d^2\hat{\mathbf{k}}_1 \int d^2\hat{\mathbf{k}}_2 Y_{\lambda_1\mu_1}^*(\hat{\mathbf{k}}_1) Y_{\lambda_2\mu_2}^*(\hat{\mathbf{k}}_2) \mathcal{S}_{\lambda_3\mu_3}(\mathbf{k}_1, \mathbf{k}_2, r), \tag{53}
 \end{aligned}$$

where we have used the inverse relation of Eq. (34).

3.2. Bispectrum from products of the first-order terms

Since only four combinations of λ_1, λ_2 , and λ_3 are non-zero, we rewrite the expression for the bispectrum, Eq. (42), as

$$B_{l_1l_2l_3} = \sum_{\lambda_1\lambda_2\lambda_3} B_{l_1l_2l_3}^{(\lambda_1,\lambda_2,\lambda_3)} + B_{l_1l_2l_3}^{Cl} = B_{l_1l_2l_3}^{(0,0,0)} + B_{l_1l_2l_3}^{(1,1,0)} + 2B_{l_1l_2l_3}^{(1,0,1)} + B_{l_1l_2l_3}^{(1,1,2)} + B_{l_1l_2l_3}^{Cl}, \tag{54}$$

where we have used $B_{l_1l_2l_3}^{(0,1,1)} = B_{l_1l_2l_3}^{(1,0,1)}$, and defined

$$B_{l_1l_2l_3}^{Cl} \equiv -3I_{l_1l_2l_3}C_{l_1}C_{l_2} + \text{cyclic}, \tag{55}$$

and

$$\begin{aligned}
 B_{l_1l_2l_3}^{(\lambda_1,\lambda_2,\lambda_3)} &\equiv \frac{2}{\pi} \sum_{\text{all}l'} \sqrt{\frac{4\pi}{(2\lambda_1+1)(2\lambda_2+1)(2\lambda_3+1)}} i^{l_3-l'_3+R} I_{l'_1l'_2l'_3} I_{l_1l'_1\lambda_1} I_{l_2l'_2\lambda_2} I_{l_3l'_3\lambda_3} \begin{Bmatrix} l_1 & l_2 & l_3 \\ l'_1 & l'_2 & l'_3 \\ \lambda_1 & \lambda_2 & \lambda_3 \end{Bmatrix} \\
 &\quad \times \int dr e^{-\tau} \prod_{i=1}^2 \int dk_i k_i^2 P_\zeta(k_i) j_{l'_i}(rk_i) g_{l_i}(k_i) \mathcal{S}_{\lambda_1\lambda_2\lambda_3}(k_1, k_2, r) + \text{perm}. \tag{56}
 \end{aligned}$$

To proceed further, we simplify the expression by introducing the following notation for the integral over k that appears many times:

$$[x]_{ll'}^{(n)}(r) \equiv \frac{2}{\pi} \int dk k^{2+n} P_\zeta(k) j_{l'}(rk) g_l(k) x(k, r). \quad (57)$$

This function corresponds to the existing functions in the literature in the appropriate limits. For example, for $x(k, r) = \pi/2$, this function is the same as $\beta_{ll'}^{(n)}(r)$ introduced in [11]. In fact, we find that an order-of-magnitude estimate of $[x]_{ll'}^{(n)}(r)$ is given by $[x]_{ll'}^{(n)}(r) \sim 2\beta_{ll'}^{(n)}(r)/\pi \times x(k = l'/r, r)$ for a smooth function of $x(k, r)$. As $\beta_{ll'}^{(n)}(r)$ is a sharply peaked function at the decoupling epoch, $r = r_*$, we find that $[x]_{ll'}^{(n)}(r)$ is also sharply peaked at $r = r_*$.

With these tools in hand, we shall calculate $B_{l_1 l_2 l_3}^{(0,0,0)}$, $B_{l_1 l_2 l_3}^{(1,1,0)}$, $B_{l_1 l_2 l_3}^{(1,0,1)}$, and $B_{l_1 l_2 l_3}^{(1,1,2)}$ in the following subsections.

3.2.1. $B_{l_1 l_2 l_3}^{(0,0,0)}$ and $B_{l_1 l_2 l_3}^{(1,1,0)}$ The contributions to the bispectrum from the second-order monopole terms at the decoupling epoch are $B_{l_1 l_2 l_3}^{(0,0,0)}$ and $B_{l_1 l_2 l_3}^{(1,1,0)}$. For the former the second-order monopole is created from products of the first-order monopole terms. For the latter it is created from products of the first-order dipole terms.

First, we calculate $B_{l_1 l_2 l_3}^{(0,0,0)}$:

$$\begin{aligned} B_{l_1 l_2 l_3}^{(0,0,0)} &= \frac{\pi}{2} \sum_{\text{all } l'} i^{l_3 - l'_3 + R} \sqrt{4\pi} I_{l'_1 l'_2 l'_3} I_{l_1 l'_1 0} I_{l_2 l'_2 0} I_{l_3 l'_3 0} \begin{Bmatrix} l_1 & l_2 & l_3 \\ l'_1 & l'_2 & l'_3 \\ 0 & 0 & 0 \end{Bmatrix} \\ &\times \int dr \left\{ -4g(r) [v_0]_{l_1 l_1}^{(0)} [i\Delta_1]_{l_2 l_2}^{(0)} + 8e^{-\tau} [\Psi']_{l_1 l_1}^{(0)} [\Delta_0]_{l_2 l_2}^{(0)} \right\} + \text{perm}, \end{aligned} \quad (58)$$

where $g(r)$ is visibility function defined by

$$g(r) = -\tau' e^{-\tau}, \quad \int_0^{\tau_0} dr g(r) = 1. \quad (59)$$

In the first term of the second line of Eq. (58), the readers might wonder why what-appears-to-be-dipole contributions, v_0 and Δ_1 , appeared. They should be interpreted as the monopole contributions, as these contributions here represent the absolute values of the bulk velocities of the electrons and the photons, respectively, rather than the dipoles. See the second term on the second line of Eq. (44), $2iv_0^{(1)} \Delta_1^{(1)} \delta_{l_0} \delta_{m_0}$, which contributes only to the monopole of the source term, $l = 0$.

Eq. (58) may be simplified further by using

$$I_{l_1 l'_1 0} = (-1)^{l_1} \sqrt{\frac{2l_1 + 1}{4\pi}} \delta_{l_1 l'_1}, \quad (60)$$

and

$$\left\{ \begin{Bmatrix} l_1 & l_2 & l_3 \\ l'_1 & l'_2 & l'_3 \\ 0 & 0 & 0 \end{Bmatrix} \right\} = \frac{\delta_{l_1 l'_1} \delta_{l_2 l'_2} \delta_{l_3 l'_3}}{\sqrt{(2l_1 + 1)(2l_2 + 1)(2l_3 + 1)}}. \quad (61)$$

We obtain

$$B_{l_1 l_2 l_3}^{(0,0,0)} = \frac{1}{2} I_{l_1 l_2 l_3} \int dr \left\{ -g(r) [v_0]_{l_1 l_1}^{(0)} [i\Delta_1]_{l_2 l_2}^{(0)} + 2e^{-\tau} [\Psi]_{l_1 l_1}^{(0)} [\Delta_0]_{l_2 l_2}^{(0)} \right\} + perm. \quad (62)$$

Next, we calculate $B_{l_1 l_2 l_3}^{(1,1,0)}$:

$$B_{l_1 l_2 l_3}^{(1,1,0)} = -\frac{\pi}{6} \sqrt{2l_3 + 1} \sum_{\text{all } l'} i^{l_1 + l_2 + l'_1 + l'_2} I_{l'_1 l'_2 l_3} I_{l_1 l'_1 1} I_{l_2 l'_2 1} \left\{ \begin{matrix} l_1 & l_2 & l_3 \\ l'_1 & l'_2 & l_3 \\ 1 & 1 & 0 \end{matrix} \right\} \\ \times \frac{4}{\sqrt{3}} \int dr \left\{ 5g(r) [v_0]_{l_1 l'_1}^{(0)} [v_0]_{l_2 l'_2}^{(0)} + 2e^{-\tau} [\Psi + \Phi]_{l_1 l'_1}^{(1)} \sum_{L=\text{odd}} (2L+1) [i\Delta_L]_{l_2 l'_2}^{(0)} \right\} + perm. \quad (63)$$

We simplify this result further by using

$$\left\{ \begin{matrix} l_1 & l_2 & l_3 \\ l'_1 & l'_2 & l_3 \\ 1 & 1 & 0 \end{matrix} \right\} = -\frac{(-1)^{l'_1 + l_2}}{\sqrt{3(2l_3 + 1)}} \left\{ \begin{matrix} l_1 & l_2 & l_3 \\ l'_2 & l'_1 & 1 \end{matrix} \right\}. \quad (64)$$

Both l'_1 and l'_2 satisfy the triangular conditions demanded by the Wigner $6j$ symbols: $l_1 - 1 \leq l'_1 \leq l_1 + 1$ and $l_2 - 1 \leq l'_2 \leq l_2 + 1$. The function $I_{l'_1 l'_2 l_3}$, which contains the Wigner $3j$ symbols of $(l'_1, l'_2, l_3; 0, 0, 0)$, requires $l'_1 + l'_2 + l_3 = \text{even}$. The other functions, $I_{l_1 l'_1 1}$ and $I_{l_2 l'_2 1}$, require $l_1 + l'_1 + 1 = \text{even}$ and $l_2 + l'_2 + 1 = \text{even}$, respectively. These requirements suggest that one may write $l'_1 - l_1 = n_1$ and $l'_2 - l_2 = n_2$, where n_1 and n_2 are always odd. With this result and the above triangular conditions, we find that n_1 and n_2 can be either $+1$ or -1 . From these results we finally obtain

$$B_{l_1 l_2 l_3}^{(1,1,0)} = \frac{2\pi}{9} \sum_{n_1, n_2 = \pm 1} i^{n_1 - n_2} I_{l'_1 l'_2 l_3} I_{l_1 l'_1 1} I_{l_2 l'_2 1} \left\{ \begin{matrix} l_1 & l_2 & l_3 \\ l'_2 & l'_1 & 1 \end{matrix} \right\} \\ \times \int dr \left\{ 5g(r) [v_0]_{l_1 l'_1}^{(0)} [v_0]_{l_2 l'_2}^{(0)} + 2e^{-\tau} [\Psi + \Phi]_{l_1 l'_1}^{(1)} \sum_{L=\text{odd}} (2L+1) [i\Delta_L]_{l_2 l'_2}^{(0)} \right\} + perm. \quad (65)$$

3.2.2. $B_{l_1 l_2 l_3}^{(1,0,1)}$ The contribution to the bispectrum from the second-order dipole terms at the decoupling epoch is $B_{l_1 l_2 l_3}^{(1,0,1)}$, which is created from products of the first-order monopole and dipole terms. We obtain

$$B_{l_1 l_2 l_3}^{(1,0,1)} = \frac{\pi}{3} \sum_{n_1, n_3 = \pm 1} i^{n_1 + 1} I_{l'_1 l'_2 l'_3} I_{l_1 l'_1 1} I_{l_3 l'_3 1} \left\{ \begin{matrix} l_1 & l_3 & l_2 \\ l'_3 & l'_1 & 1 \end{matrix} \right\} \\ \times \int dr \left\{ -g(r) [v_0]_{l_1 l'_1}^{(0)} [4\delta_e + 4\Phi + 2\Delta_0 - \Delta_2]_{l_2 l_2}^{(0)} \right. \\ \left. + 4e^{-\tau} [\Phi]_{l_1 l'_1}^{(1)} [\Delta_0 - \Psi]_{l_2 l_2}^{(0)} + e^{-\tau} [\Delta_0]_{l_1 l'_1}^{(1)} [\Psi + \Phi]_{l_2 l_2}^{(0)} \right\} + perm, \quad (66)$$

where $l'_1 = l_1 + n_1$ and $l'_3 = l_3 + n_3$.

3.2.3. $B_{l_1 l_2 l_3}^{(1,1,2)}$ The contribution to the bispectrum from the second-order quadrupole terms at the decoupling epoch is $B_{l_1 l_2 l_3}^{(1,1,2)}$, which is created from products of the first-order

dipole terms. We obtain

$$\begin{aligned}
 B_{l_1 l_2 l_3}^{(1,1,2)} &= \frac{2}{3\pi} \sqrt{\frac{4\pi}{5}} (-1)^{l_3} \sum_{\text{all } l'} i^{l_1+l_2+l'_1+l'_2} I_{l'_1 l'_2 l'_3} I_{l_1 l'_1 1} I_{l_2 l'_2 1} I_{l_3 l'_3 2} \left\{ \begin{matrix} l_1 & l_2 & l_3 \\ l'_1 & l'_2 & l'_3 \\ 1 & 1 & 2 \end{matrix} \right\} \\
 &\times 2\sqrt{\frac{10}{3}} \int dr \left\{ -7g(r) [v_0]_{l_1 l'_1}^{(0)} [v_0]_{l_2 l'_2}^{(0)} - e^{-\tau} [\Psi + \Phi]_{l_1 l'_1}^{(1)} \sum_{L=\text{odd}} (2L+1) [i\Delta_L]_{l_2 l'_2}^{(0)} \right\} \\
 &+ \text{perm}, \tag{67}
 \end{aligned}$$

where l'_1 , l'_2 , and l'_3 satisfy the triangular conditions: $l_1 - 1 \leq l'_1 \leq l_1 + 1$, $l_2 - 1 \leq l'_2 \leq l_2 + 1$, and $l_3 - 2 \leq l'_3 \leq l_3 + 2$, which yields the conditions on $n_1 = l'_1 - l_1$, $n_2 = l'_2 - l_2$, and $n_3 = l'_3 - l_3$ as $-1 \leq n_1 \leq 1$, $-1 \leq n_2 \leq 1$, and $-2 \leq n_3 \leq 2$.

The Wigner $3j$ symbols in $I_{l'_1 l'_2 l'_3}$, $I_{l_1 l'_1 1}$, $I_{l_2 l'_2 1}$, and $I_{l_3 l'_3 2}$ require $n_1 = \text{odd}$, $n_2 = \text{odd}$, $n_3 = \text{even}$, and $l_1 + l_2 + l_3 = \text{even}$; thus, only $n_1, n_2 = \pm 1$ and $n_3 = \pm 2, 0$ are allowed. We finally obtain

$$\begin{aligned}
 B_{l_1 l_2 l_3}^{(1,1,2)} &= -\frac{8}{9} \sqrt{\frac{6}{\pi}} \sum_{n_1, n_2 = \pm 1} \sum_{n_3 = \pm 2, 0} i^{n_1+n_2} I_{l'_1 l'_2 l'_3} I_{l_1 l'_1 1} I_{l_2 l'_2 1} I_{l_3 l'_3 2} \left\{ \begin{matrix} l_1 & l_2 & l_3 \\ l'_1 & l'_2 & l'_3 \\ 1 & 1 & 2 \end{matrix} \right\} \\
 &\times \int dr \left\{ 7g(r) [v_0]_{l_1 l'_1}^{(0)} [v_0]_{l_2 l'_2}^{(0)} + e^{-\tau} [\Psi + \Phi]_{l_1 l'_1}^{(1)} \sum_{L=\text{odd}} (2L+1) [i\Delta_L]_{l_2 l'_2}^{(0)} \right\} + \text{perm}. \tag{68}
 \end{aligned}$$

4. Shape and signal-to-noise of the second-order bispectrum from products of the first-order terms

One of the motivations for calculating the second-order bispectrum is to see how much the second-order effects in gravity and the photon-baryon fluid contaminate the extraction of the primordial bispectrum. If, for example, the predicted shape of the second-order bispectrum is sufficiently different from that of the primordial bispectrum, then one would hope that the contamination would be minimal. To investigate this, we shall compare the numerical results of the second-order bispectrum with the so-called ‘‘local’’ model of the primordial bispectrum.

We extract the first-order perturbations from the CMBFAST code [22]. We use the following cosmological parameters: $\Omega_\Lambda = 0.72$, $\Omega_m = 0.23$, $\Omega_b = 0.046$, $h = 0.70$, and assume a power law spectrum, $P_\zeta \propto k^{n-4}$, with $n = 1$. We determine the decoupling time, η_* , from the peak of the visibility function. In this model we have $c\eta_0 = 14.9$ Gpc and $c\eta_* = 288$ Mpc. While the most of the signal is generated in the region of the decoupling epoch, in the low- l regime we must also take into account the late time contribution due to the late integrated Sachs-Wolfe effect; thus, we integrate over the line-of-sight, r , in the following regions: $c(\eta_0 - 5\eta_*) < r < c(\eta_0 - 0.7\eta_*)$ for $l > 100$, and $0 < r < c(\eta_0 - 0.7\eta_*)$ for $l \leq 100$. The step size is $\Delta r = 0.1\eta_*$ around the decoupling epoch, and we use the same time steps used by CMBFAST after the decoupling epoch.

The local primordial bispectrum is given by [10]

$$B_{l_1 l_2 l_3} = 2I_{l_1 l_2 l_3} \int_0^\infty r^2 dr b_{l_1}^L(r) b_{l_2}^L(r) b_{l_3}^{NL}(r) + \text{cyclic}, \quad (69)$$

where

$$\begin{aligned} b_i^L(r) &\equiv \frac{2}{\pi} \int_0^\infty k^2 dk P_\Phi(k) g_{Ti}^{\text{KS}}(k) j_l(kr), \\ b_i^{NL}(r) &\equiv \frac{2}{\pi} \int_0^\infty k^2 dk f_{NL} g_{Ti}^{\text{KS}}(k) j_l(kr). \end{aligned} \quad (70)$$

Note that our linear transfer function, $g_l(k)$, is related to that of [10], $g_{Ti}^{\text{KS}}(k)$, by $g_l(k) = \frac{3}{5} g_{Ti}^{\text{KS}}(k)$.

Figure 1 shows a shape of the bispectrum generated by the products of the first-order terms, and compares it to the primordial bispectrum, for $l_3 = 200$. Both shapes (second-order and primordial) have the largest signals in the squeezed triangles, $l_1 \ll l_2 \approx l_3$. This is an expected result: the local primordial bispectrum arises from the primordial curvature perturbation in position space written as $\zeta(\mathbf{x}) = \zeta_L(\mathbf{x}) + \frac{3}{5} f_{NL} \zeta_L^2(\mathbf{x})$, where ζ_L is a Gaussian perturbation. The second-order bispectrum that we have computed here arises from the products of the first-order terms, also products in position space. However, these two shapes are slightly different when l_1/l_3 is not so small ($l_1/l_3 = \mathcal{O}(0.1)$): the ways in which the radiation transfer function (which gives the acoustic oscillations) enters into the bispectrum are different for the products of the first-order terms and the primordial bispectrum. The primordial bispectrum contains $j_l(kr_*) g_l(k)$, whereas the second-order bispectrum contains $j_l(kr_*) g_l(k) x(k, r_*)$ where $x = \Delta_0, v_0$, etc., also has the oscillations. Therefore, the second-order bispectrum has more interferences between multiple radiation transfer functions. Moreover, the second-order effects contain derivatives that the local primordial effects do not have, which also makes the details of the two shapes different.

Notice, in particular, that most of these gradients in the source term, Eq. (44), are contracted with the direction vector, $\hat{\mathbf{n}}$. There is only one term that has a scalar product of two wave-vectors, $\mathbf{k}_1 \cdot \mathbf{k}_2$, which vanishes in the squeezed limit. The resulting bispectrum, Eq. (54), resembles that of a local form, except for the extra powers of k coming from the derivatives. These extra powers of k will affect the scale-dependence of the bispectrum, i.e., the second-order bispectrum is no longer scale-invariant. Nevertheless, the largest signal of the bispectrum still comes from the squeezed configurations, as the number of extra powers of k from the derivatives in the source term is not large enough to change the fact that we have the largest contribution when one of k_1, k_2 , and k_3 is very small. In other words, schematically the bispectrum looks like $B(k_1, k_2, k_3) \sim (k_1^{m_1} k_2^{m_2}) / (k_1^3 k_2^3) + \text{cyclic}$, where m_1 and m_2 are the extra powers of k from the derivatives. Therefore, the largest contribution is in the squeezed configurations as long as $m_i < 3$.

Figure 2 shows the same for $l_3 = 1000$. The results are similar to those for $l_3 = 200$, but the acoustic oscillations are more clearly visible.

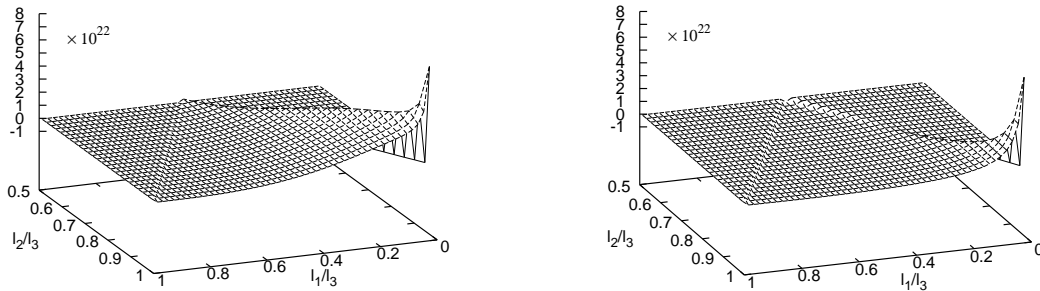


Figure 1. Shape dependence of the second-order bispectrum from products of the first-order terms (top) and that of the local primordial bispectrum (bottom). We show $l_1 l_2 \langle a_{l_1 m_1}^{(1)} a_{l_2 m_2}^{(1)} a_{l_3 m_3}^{(2)} \rangle (\mathcal{G}_{l_1 l_2 l_3}^{m_1 m_2 m_3})^{-1} / (2\pi)^2 \times 10^{22}$ as a function of l_1/l_3 and l_2/l_3 where $l_3 = 200$. Both shapes have the largest signals in the squeezed triangles, $l_1 \ll l_2 \approx l_3$.

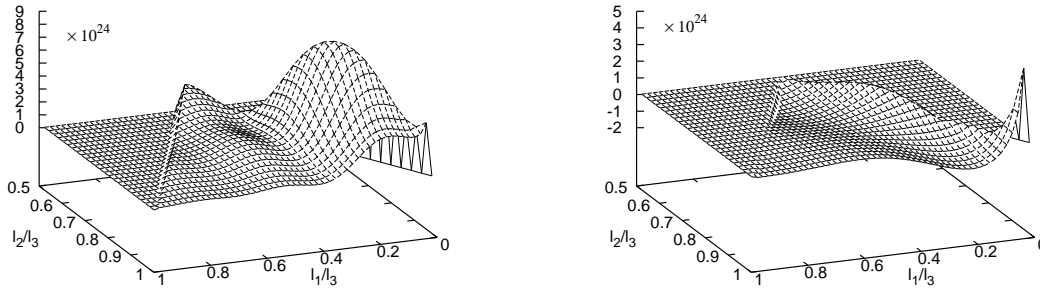


Figure 2. Same as Fig. 1 for $l_3 = 1000$. The acoustic oscillations are clearly seen.

How similar are the second-order and the primordial bispectra? What is the contamination level? We shall quantify the degree to which these spectra are correlated, as well as the expected signal-to-noise ratio of the second-order bispectrum, following the standard method given in [10]. Namely, the Fisher matrix for the amplitudes of the bispectra, F_{ij} , is given by

$$F_{ij} \equiv \sum_{2 \leq l_1 \leq l_2 \leq l_3} \frac{B_{l_1 l_2 l_3}^{(i)} B_{l_1 l_2 l_3}^{(j)}}{\sigma_{l_1 l_2 l_3}^2}, \quad (71)$$

where

$$\sigma_{l_1 l_2 l_3}^2 \equiv \langle B_{l_1 l_2 l_3}^2 \rangle - \langle B_{l_1 l_2 l_3} \rangle^2 \approx C_{l_1} C_{l_2} C_{l_3} \Delta_{l_1 l_2 l_3}, \quad (72)$$

and $\Delta_{l_1 l_2 l_3}$ takes values 1, 2, and 6 when all l 's are different, two of them are equal and all are the same, respectively. The power spectrum, C_l , is the sum of the theoretical CMB and the detector noise. Throughout this paper we shall ignore the noise contribution.

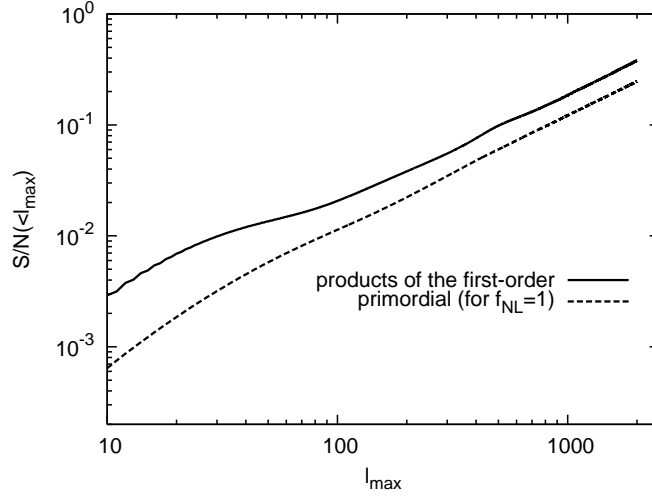


Figure 3. Signal-to-noise ratios for the local primordial bispectrum for $f_{NL} = 1$ (dashed), and the second-order bispectrum from the products of the first-order terms (solid), for an ideal full-sky and cosmic-variance-limited (noiseless) experiment.

In other words, we shall only consider ideal cosmic-variance limited experiments with full sky coverage.

The signal-to-noise ratio is given by

$$\left(\frac{S}{N}\right)_i = \frac{1}{\sqrt{F_{ii}^{-1}}}, \quad (73)$$

and we define the cross-correlation coefficient between different shapes i and j , r_{ij} , as

$$r_{ij} \equiv \frac{F_{ij}}{\sqrt{F_{ii}F_{jj}}}. \quad (74)$$

In Fig. 3 we show the cumulative signal-to-noise ratio, summed up to a maximum multipole of l_{max} , of the primordial bispectrum, assuming $f_{NL} = 1$ and ignoring the second-order bispectrum, i.e., $(S/N)_{prim} = (F_{prim,prim})^{1/2}$, as well as that of the second-order bispectrum, ignoring the primordial bispectrum, i.e., $(S/N)_{2nd} = (F_{2nd,2nd})^{1/2}$. In both cases S/N increases roughly as $S/N \propto l_{max}$ (or $\propto \sqrt{N_{pix}}$ where N_{pix} is the number of independent pixels in the map). A larger contribution to the second-order bispectrum at $l \lesssim 50$ comes from the terms involving the Integrated Sachs-Wolfe effect. The signal-to-noise ratio of the second-order bispectrum reaches ~ 0.4 at $l_{max} = 2000$; thus, this signal is undetectable. While our calculation includes the temperature anisotropy only, including polarization would increase the signal-to-noise by a factor of two at most, which would not be enough to push the signal-to-noise above unity.

While the total signal-to-noise does not exceed unity, it may still be instructive to show which terms of $B_{l_1 l_2 l_3}^{(\lambda_1, \lambda_2, \lambda_3)}$ and $B_{l_1 l_2 l_3}^{C_i}$ are more important than the others. To do this we show the following quantity:

$$\left(\frac{S}{N}\right)_{ab} \equiv \left| \sum_{2 \leq l_1 \leq l_2 \leq l_3} \frac{B_{l_1 l_2 l_3}^a B_{l_1 l_2 l_3}^b}{\sigma_{l_1 l_2 l_3}^2} \right|^{1/2}, \quad (75)$$

where $a, b = 1, 2, 3, 4$, and 0 correspond to $(0, 0, 0)$, $(1, 1, 0)$, $(1, 0, 1)$, $(1, 1, 2)$, and C_l , respectively.

The results are shown in Fig. 4. We find that $(S/N)_{2nd}$ is dominated by $B_{l_1 l_2 l_3}^{(\lambda_1, \lambda_2, \lambda_3)}$ for $l \lesssim 100$, whereas it is dominated by $B_{l_1 l_2 l_3}^{C_l}$ for $l \gtrsim 100$ (see the top panel).

Among $B_{l_1 l_2 l_3}^{(\lambda_1, \lambda_2, \lambda_3)}$, the most dominant term is $(1, 0, 1)$ (the bispectrum from the second-order dipole created by the first-order dipole and monopole). The second most dominant is $(0, 0, 0)$ (from the second-order monopole created by the first-order monopole) for $l \lesssim 400$ and $(1, 1, 0)$ (from the second-order monopole created by the first-order dipole) for $l \gtrsim 400$. The cross terms (middle and bottom panels) are sub-dominant compared to the auto terms (top panel) at all multipoles.

How similar are the second-order and the primordial bispectra? In Fig. 5 we show the cross-correlation coefficient between the second-order bispectrum from the products of the first-order terms and the local primordial bispectrum. The cross-correlation coefficient reaches ~ 0.5 for $l_{max} = 200$, and the shapes for $l_3 = 200$ are shown in Fig. 1. After $l_{max} = 200$ the correlation weakens, and reaches ~ 0.35 at $l_{max} = 1000$, and the shapes for $l_3 = 1000$ are shown in Fig. 2. These results show that the second-order bispectrum from the products of the first-order perturbations and the local primordial bispectrum are fairly similar, with a sizable correlation coefficient. The next question is, ‘‘how large is the contamination of the primordial bispectrum?’’

We quantify the contamination of the primordial bispectrum due to the second-order effects from the products of the first-order perturbations as follows: we fit the primordial bispectrum template to the second-order bispectrum, and find the best-fitting f_{NL}^{con} (‘‘con’’ stands for contamination) by minimizing χ^2 given by

$$\chi^2 = \sum_{2 \leq l_1 \leq l_2 \leq l_3} \frac{(f_{NL} B_{l_1 l_2 l_3}^{prim} - B_{l_1 l_2 l_3}^{2nd})^2}{\sigma_{l_1 l_2 l_3}^2}, \quad (76)$$

with respect to f_{NL} . Here, $B_{l_1 l_2 l_3}^{prim}$ is the local-type primordial bispectrum with $f_{NL} = 1$ [10]. We obtain

$$\begin{aligned} f_{NL}^{con} &= \frac{1}{N} \sum_{2 \leq l_1 \leq l_2 \leq l_3} \frac{B_{l_1 l_2 l_3}^{2nd} B_{l_1 l_2 l_3}^{prim}}{\sigma_{l_1 l_2 l_3}^2}, \\ N &= \sum_{2 \leq l_1 \leq l_2 \leq l_3} \frac{(B_{l_1 l_2 l_3}^{prim})^2}{\sigma_{l_1 l_2 l_3}^2}. \end{aligned} \quad (77)$$

This is the value of f_{NL} one would find, if one did not know that the primordial bispectrum did not exist but there was only the second-order bispectrum from the products of the first-order terms. In Fig. 6 we show f_{NL}^{con} as a function of the maximum multipoles, l_{max} . We find that f_{NL}^{con} reaches the maximum value, ~ 0.9 , when the correlation coefficient reaches the maximum at $l_{max} \sim 200$, but then decreases to ~ 0.5 at $l_{max} \sim 2000$. Therefore, we conclude that the contamination of the primordial bispectrum due to the second-order bispectrum is negligible for CMB experiments.

Finally, we calculate the $1\text{-}\sigma$ uncertainty of f_{NL} , Δf_{NL} , with the second-order

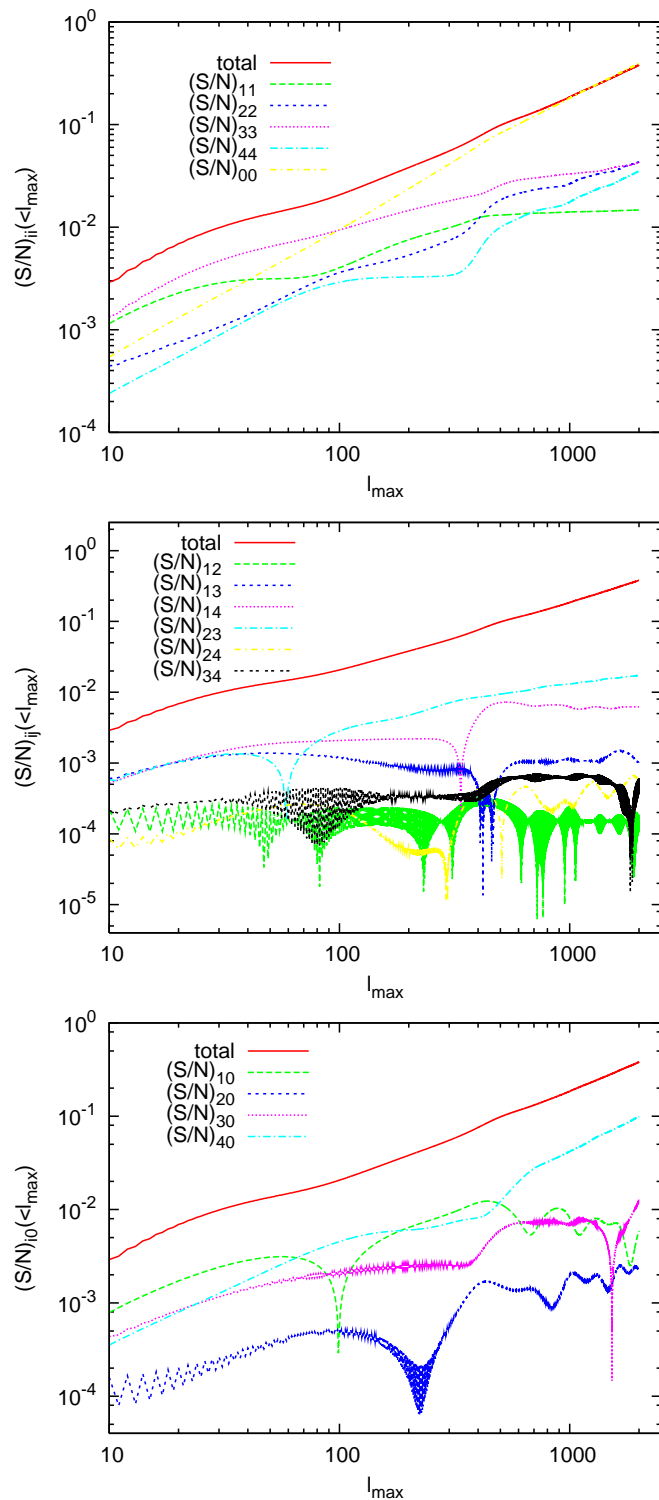


Figure 4. Absolute values of the contributions to the signal-to-noise ratio from each component, $(S/N)_{ab}$, as defined by Eq. (75).

bispectrum marginalized over. This is given by $\Delta f_{NL} = \sqrt{(F^{-1})_{prim,prim}}$. Fig. 7 shows that an increase in the uncertainty of f_{NL} due to marginalization is totally negligible.

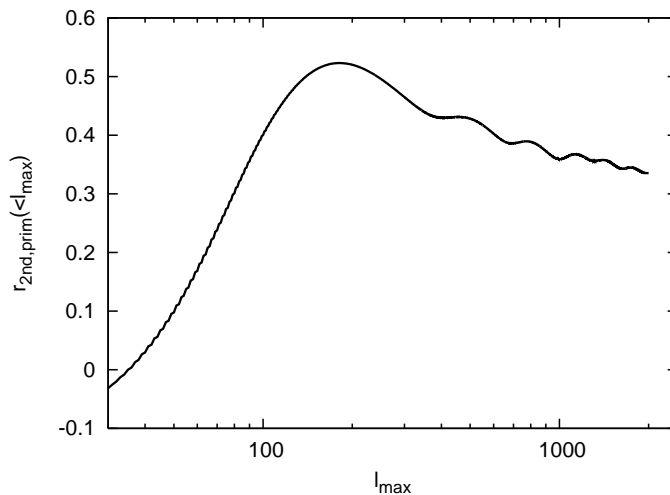


Figure 5. The cross-correlation coefficient between the second-order bispectrum from the products of the first-order terms and the local primordial bispectrum.

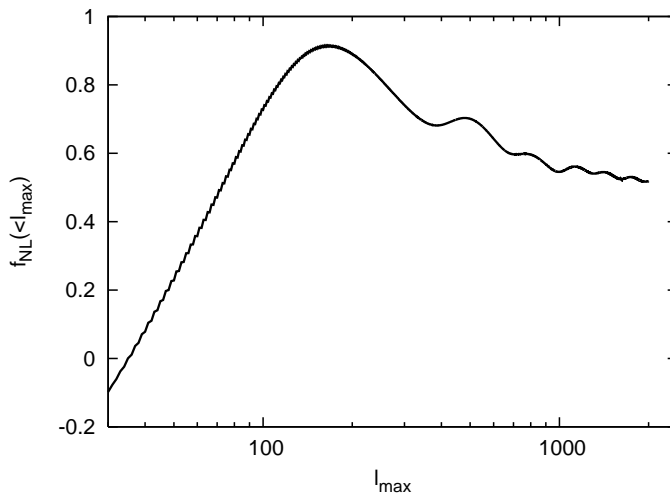


Figure 6. Contamination of the local primordial bispectrum as measured by f_{NL}^{con} (Eq (77)).

5. Conclusions

We have presented the general formula of the CMB angular averaged bispectrum, Eq. (42), arising from the source terms that contain second-order perturbations in the Boltzmann equation, Eq. (44). In this paper we have considered the source terms that are products of the first-order perturbations. Since they are products in position space, similar to the local primordial non-Gaussianity, the predicted shapes of the angular bispectrum from the products of the first-order terms are similar to those of the local-type primordial bispectrum, with cross-correlation coefficients of ~ 0.5 and 0.35 for $l_{max} \sim 200$ and 1000 , respectively.

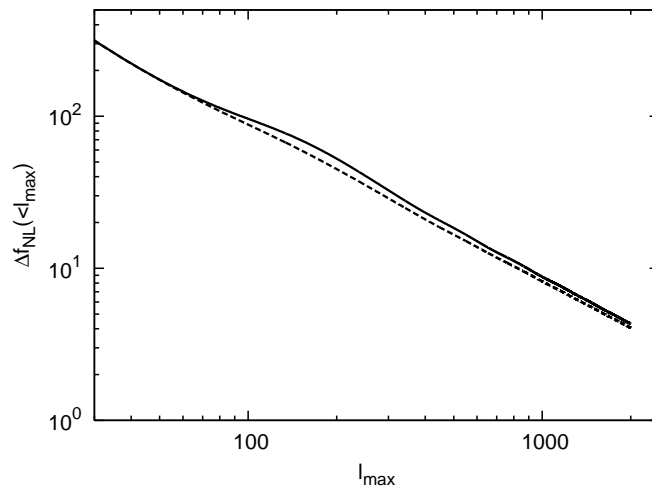


Figure 7. Projected uncertainty of f_{NL} with (dashed) and without (solid) the second-order bispectrum marginalized over.

The predicted signal-to-noise ratio of the products of the first-order perturbations is small: it reaches only up to $S/N \sim 0.4$ for $l_{max} = 2000$, even with an ideal cosmic-variance-limited experiment. The contamination of the local primordial bispectrum is minimal: the contamination, f_{NL}^{con} , is only 0.9 for $l_{max} = 200$ and 0.5 for $l_{max} = 2000$, and an increase in the uncertainty in f_{NL} due to marginalization over the second-order bispectrum is negligible. This level of the contamination is completely negligible for the present analysis of the WMAP data [23, 9]. The contamination is negligible also for the Planck data, for which the expected $1-\sigma$ uncertainty is $\Delta f_{NL} \sim 5$, or even for the ideal experiment, for which $\Delta f_{NL} \sim 3$ [10]. Therefore, we conclude that the effects of the products of the first-order perturbations in the Boltzmann equation may be safely ignored when one tries to extract f_{NL} from the CMB temperature data.

We shall present the numerical calculations of the bispectrum that include the contributions from the intrinsically second-order terms as well as those from the perturbed recombination, both of which were ignored in this paper, in future publications.

Acknowledgments

D. N. would like to thank Toshifumi Futamase for helpful discussions. This work is supported in part by NSF grant PHY-0758153 and the Grant-in-Aid for Tohoku University Global Center of Excellence (GCOE) Program, “Weaving Science Web beyond Particle-Matter Hierarchy,” from the Ministry of Education, Culture, Sports, Science and Technology (MEXT) of Japan. E. K. acknowledges support from the Alfred P. Sloan Foundation. N.B. and S.M. acknowledge partial financial support by ASI, under contracts I/016/07/0 “COFIS” and Planck LFI Activity of Phase E2.

Reference

- [1] N. Bartolo, E. Komatsu, S. Matarrese and A. Riotto, Phys. Rept. **402**, 103 (2004) .
- [2] E. Komatsu, ph.D. thesis at Tohoku University arXiv:astr-ph/0206039 .
- [3] D. H. Lyth, C. Ungarelli and D. Wands, Phys. Rev. D **67**, 23503 (2003) .
- [4] D. Babich, P. Creminelli and M. Zaldarriaga, JCAP **0408**, 009 (2004) .
- [5] X. Chen, M.-x. Huang, S. Kachru and G. Shiu, JCAP **0701**, 002 (2007) .
- [6] R. Holman and A. J. Tolley, JCAP **0805**, 001 (2008) .
- [7] J. M. Maldacena, JHEP **05**, 013 (2003) .
- [8] V. Acquaviva, N. Bartolo, S. Matarrese and A. Riotto, Nucl. Phys. B **667**, 119 (2003) .
- [9] K. Smith, L. Senatore and M. Zaldarriaga, arXiv:0901.2572 [astro-ph] .
- [10] E. Komatsu and D.N.Spergel, Phys. Rev. D **63**, 063002 (2001) .
- [11] M. Liguori, E. Komatsu, S. Matarrese and A. Riotto, Phys. Rev. D **73**, 043505 (2006) .
- [12] N. Bartolo, S. Matarrese and A. Riotto, JCAP **0606**, 024 (2006) .
- [13] N. Bartolo, S. Matarrese and A. Riotto, JCAP **0701**, 019 (2007) .
- [14] C. Pitrou, Class. Quant. Grav. **24**, 6127 (2007); C. Pitrou, Class. Quant. Grav. **26**, 065006 (2009);
C. Pitrou, arXiv:0809.3245 [astro-ph]
- [15] N. Bartolo, S. Matarrese and A. Riotto, JCAP **0605**, 010 (2006) .
- [16] C. Pitrou, J.-P. Uzan and F. Bernardeau, Phys. Rev. D **78**, 063526 (2008) .
- [17] N. Bartolo and A. Riotto, arXiv:0811.4584 [astro-ph] .
- [18] R. Khatri and B. Wandelt, Phys. Rev. D **79**, 023501 (2009) .
- [19] L. Senatore, S. Tassev and M. Zaldarriaga, arXiv:0812.3652v1 [astro-ph] .
- [20] L. Senatore, S. Tassev and M. Zaldarriaga, arXiv:0812.3658v1 [astro-ph] .
- [21] N. Bartolo, S. Matarrese and A. Riotto, arXiv:astr-ph/0703496 .
- [22] U. Seljak and M. Zaldarriaga, Astrophys. J. **469**, 437-444 (1996) .
- [23] E. Komatsu *et al.*, Astrophys. J. S. **180**, 330 (2009) .